Available online at www.sciencedirect.com
ScienceDirect
Journal of Solid State Chemistry 180 (2007) 1764–1769
JOURNAL OF SOLID STATE CHEMISTRY
www.elsevier.com/locate/jssc

Synthesis, crystal and band structures, and optical properties of a new lanthanide–alkaline earth tellurium(IV) oxide: $La_2Ba(Te_3O_8)(TeO_3)_2$

Hai-Long Jiang[a,b], Fang Kong[a,b], Jiang-Gao Mao[a,*]

[a]*State Key Laboratory of Structural Chemistry, Fujian Institute of Research on the Structure of Matter, Chinese Academy of Sciences, Fuzhou 350002, PR China*
[b]*Graduate School of the Chinese Academy of Sciences, Beijing 100039, PR China*

Received 24 February 2007; received in revised form 4 April 2007; accepted 4 April 2007
Available online 10 April 2007

Abstract

A new quaternary lanthanide alkaline–earth tellurium(IV) oxide, $La_2Ba(Te_3O_8)(TeO_3)_2$, has been prepared by the solid-state reaction and structurally characterized. The compound crystallizes in monoclinic space group $C2/c$ with $a = 19.119(3)$, $b = 5.9923(5)$, $c = 13.2970(19)$ Å, $\beta = 107.646(8)^\circ$, $V = 1451.7(3)$ Å^3 and $Z = 4$. $La_2Ba(Te_3O_8)(TeO_3)_2$ features a 3D network structure in which the cationic $[La_2Ba(TeO_3)_2]^{4+}$ layers are cross-linked by $Te_3O_8^{4-}$ anions. Both band structure calculation by the DFT method and optical diffuse reflectance spectrum measurements indicate that $La_2Ba(Te_3O_8)(TeO_3)_2$ is a wide band-gap semiconductor.

Keywords: Solid state reaction; Crystal structure; Band structure; La–Ba tellurium(IV) oxide; Optical properties

1. Introduction

Metal selenites and tellurites can form a variety of unusual structures because of the presence of the stereochemically active lone pair electrons which may serve as an invisible structure-directing agent [1]. Much more structural types are available for metal tellurites since Te(IV) can be coordinated by three, four or five oxygen atoms and the TeO_x ($x = 3$, 4, 5) polyhedra can be interconnected into a variety of polymeric tellurium(IV) oxide anions with extended structures under solid state reactions at high temperature ($T > 600\,^\circ$C) [2] or supercritical hydrothermal conditions [3]. The asymmetric coordination polyhedron adopted by Se(IV) or Te(IV) atom may also result in non-centrosymmetric structures with consequent interesting physical properties, such as nonlinear optical second harmonic generation (SHG) [4–6]. Furthermore, transition metal Se(IV) or Te(IV) oxyhalides can be regarded as "chemical scissors" since the effective volume of the lone pair is approximately the same as the volume of an O^{2-} ion, and they are promising new low-dimensional magnets [7]. So far, a number of lanthanide tellurites and a few lanthanide selenites or tellurium(IV) oxides with additional transition metal ions have been reported [1,8–10]. We deem that the introduction of alkaline-earth metal ions into the lanthanide tellurites or selenites systems may result in new compounds with novel structures and interesting optical properties such as second-order non-linear optical properties. A literature search indicates that so far only several lanthanide alkaline earth tellurium(VI) oxides have been structurally characterized, namely, $AA'Ln TeO_6$ (A = Li, Na; A' = Mg, Ca, Sr, Ba and Ln = La, Pr, Eu) [11], and no corresponding Te(IV) compounds has been reported. Our exploration on new phases in La–Ba–Cu–Te–O system afforded the first lanthanide–alkaline earth tellurium(IV) oxide, namely, $La_2Ba(Te_3O_8)(TeO_3)_2$. Herein we report its synthesis, crystal and band structures as well as optical properties.

2. Experimental

2.1. Materials and instrumentation

All chemicals were obtained from commercial sources and used without further purification. IR spectrum was

*Corresponding author. Fax: +86 591 8371 4946.
E-mail address: mjg@fjirsm.ac.cn (J.-G. Mao).

0022-4596/$ - see front matter © 2007 Elsevier Inc. All rights reserved.
doi:10.1016/j.jssc.2007.04.002

recorded on a Magna 750 FT-IR spectrometer photometer as a KBr pellet in the 4000–400 cm^{-1}. The chemical composition of the compound was confirmed by a field emission scanning electron microscope (FESEM, JSM6700F) equipped with an energy dispersive X-ray spectroscope (EDS, Oxford INCA). X-ray powder diffraction (XRD) patterns (CuKα) were collected on a XPERT-MPD $\theta-2\theta$ diffractometer. Optical diffuse reflectance spectrum was measured at room temperature with a PE Lambda 900 UV–vis spectrophotometer. The instrument was equipped with an integrating sphere and controlled by a personal computer. The samples were ground into fine powder and pressed into a thin glass slide holder. The $BaSO_4$ plate was used as a standard (100% reflectance). The absorption spectrum was calculated from reflectance spectra using the Kubelka–Munk function: $\alpha/S=(1-R)^2/2R$ [12], where α is the absorption coefficient, S is the scattering coefficient which is practically wavelength independent when the particle size is larger than 5 μm, and R is the reflectance. Thermogravimetric analyses (TGA) were carried out with a NETZSCH STA 449C unit, at a heating rate of 10 °C/min under a static air atmosphere. Photoluminescence analysis was performed on a Perkin-Elmer LS55 fluorescence spectrometer.

2.2. Synthesis

The title compound was initially obtained by the high temperature solid state reaction of La_2O_3 (48.9 mg, 0.15 mmol), BaO (92.0 mg, 0.60 mmol), Cu_2O (21.5 mg, 0.15 mmol), and TeO_2 (191.5 mg, 1.2 mmol) in our attempt to synthesize a new Y–Ba–Cu–TeO_3 phase. The reaction mixture was thoroughly ground and pressed into a pellet, which was put into a silica tube, evacuated and sealed. The tube was heated at 720 °C for 7 days and then cooled to 300 °C at 3.5 °C/h before switching off the furnace. Colorless prism-shaped crystals of $La_2Ba(Te_3O_8)(TeO_3)_2$ were obtained. Results of energy-dispersive spectrometry (EDS) microprobe elemental analyses on single crystals of $La_2Ba(Te_3O_8)(TeO_3)_2$ gave a molar ratio of 2.1:1.0:5.2 for La:Ba:Te, and no Cu element was detected, which is in good agreement with the one determined from single crystal X-ray structure analysis. After proper structural analysis, a pure powder sample of $La_2Ba(Te_3O_8)(TeO_3)_2$ was prepared quantitatively by reacting a mixture of La_2O_3:BaO:TeO_2 in a molar ratio of 1:1:4 at 720 °C for 6 days in a sealed silica tube. The measured XRD powder pattern matches well with the one simulated from single crystal structure data (See Supporting Materials). IR data (KBr, cm^{-1}): 788 (vs), 755 (vs), 726 (vs), 687 (vs), 616 (vs), 439 (s).

2.3. Crystal structure determination

The data collection for $La_2Ba(Te_3O_8)(TeO_3)_2$ was performed on Rigaku Mercury CCD (MoKα radiation, graphite monochromator) at 293(2) K. The data were corrected for Lorentz factors, polarization, air absorption, and absorption due to variations in the path length through the detector faceplate. Absorption correction based on a multi-scan technique was also applied [13]. The space group was determined to be $C2/c$ (no. 15) based on systematic absences, E-value statistics, and subsequent successful refinements of the crystal structure. The structure itself was solved by direct methods (SHELXTL) and refined by least-squares methods with atomic coordinates and anisotropic thermal displacement parameters [13]. The crystallographic data collection and refinement parameters are summarized in Table 1. Selected bond lengths are listed in Table 2. Further details of the crystal structure investigations can be obtained from the Fachinformationszentrum Karlsruhe, 76344 Eggenstein-Leopoldshafen, Germany (fax: (49) 7247-808-666; e-mail: crysdata@fiz-karlsruhe.de), on quoting the depository numbers CSD-417616.

2.4. Computational details

Single crystal structural data of the title compound were used for the theoretical calculations. Band structure calculations along with density of states (DOS) were carried out with density functional theory (DFT) using one of the non-local gradient-corrected exchange–correlation functionals (GGA-PBE) and performed with the CASTEP code [14,15], which uses a plane wave basis set for the valence electrons and norm-conserving pseudopotential [16] for the core electrons. Pseudoatomic calculations were performed for O-$2s^2 2p^4$, Te-$5s^2 5p^4$, Ba-$5s^2 5p^6 6s^2$ and La-$5d^1 6s^2$. The parameters used in the calculations and convergence criteria were set by the default values of the

Table 1
Summary of crystal data and structure refinement for $La_2Ba(Te_3O_8)(TeO_3)_2$

Empirical formula	$BaLa_2O_{14}Te_5$
F_w	1277.16
Space group	$C2/c$ (no. 15)
a (Å)	19.119(3)
b (Å)	5.9923(5)
c (Å)	13.2970(2)
β (deg)	107.646(8)
V (Å^3)	1451.7(3)
Z	4
D_{calcd} (g cm^{-3})	5.844
μ (MoKα) (mm^{-1})	18.380
Crystal size (mm)	$0.15\times0.05\times$ 0.02
F (000)	2168
Reflections collected	5305
Independent reflections	1663 ($R_{int}=0.0377$)
Observed data [$I>2\sigma(I)$]	1411
Data/restraints/parameters	1663/0/103
GOF on F^2	1.143
R_1, wR_2 ($I>2\sigma(I)$)[a)]	0.0382/0.0804
R_1, wR_2 (all data)[a)]	0.0500/0.0870

$R_1=\sum||F_o|-|F_c||/\sum|F_o|$, $wR_2=\sum w[(F_o)^2-(F_c)^2]^2/\sum w[(F_o)^2]^{21/2}$.

Table 2
Selected bond lengths (in Å) for $La_2Ba(Te_3O_8)(TeO_3)_2$

La(1)–O(5)	2.420(7)	La(1)–O(2)	2.503(7)
La(1)–O(1)	2.515(6)	La(1)–O(4)	2.527(6)
La(1)–O(6)	2.542(6)	La(1)–O(7)	2.569(6)
La(1)–O(6)	2.626(6)	La(1)–O(7)	2.657(6)
Ba(1)–O(6)	2.730(6) × 2	Ba(1)–O(1)	2.772(6) × 2
Ba(1)–O(7)	2.784(6) × 2		
Te(1)–O(1)	1.860(7)	Te(1)–O(2)	1.862(6)
Te(1)–O(3)	1.893(6)	Te(2)–O(4)	1.850(6) × 2
Te(2)–O(3) × 2	2.179(7)	Te(3)–O(5)	1.827(7)
Te(3)–O(6)	1.890(6)	Te(3)–O(7)	1.891(6)

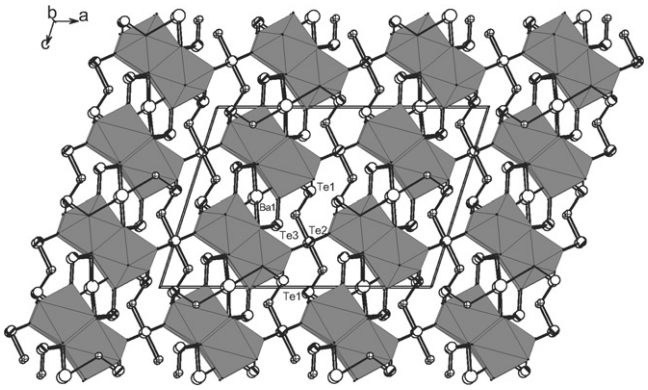

Fig. 1. View of the crystal structure of $La_2Ba(Te_3O_8)(TeO_3)_2$ down the *b*-axis. The LaO_8 polyhedra are shaded in middle gray. Ba, Te and O atoms are represented by open (large), hatched and crossed circles, respectively.

CASTEP code [14], e.g., reciprocal space pseudopotentials representations and eigen-energy convergence tolerance of 0.6567E−06 eV. The dependences of the total energy on the cutoff energy and the *k*-point set mesh according to the Monkhorst–Pack grid were studied (see Supporting Information). If the *k*-point set mesh is fixed to be $4 \times 4 \times 2$, the change of the total energy is less than 0.07 eV when the cutoff energy is increased from 450 to 600 eV; on the other hand, if cutoff energy is fixed to be 450 eV, the change of the total energy is very small when the *k*-point set mesh is changed from $4 \times 4 \times 2$ to $5 \times 5 \times 4$. For the sake of computational cost, we choose a cutoff energy of 450 eV and a Monkhorst–Pack grid of $4 \times 4 \times 2$. The calculations of linear optical properties were also made in this work. The imaginary part of the dielectric function, $\varepsilon_2(\omega)$, is given by the following equation:

$$\varepsilon_2(q \to O_{\hat{u}}, \hbar\omega) = \frac{2e^2\pi}{\Omega\varepsilon_0} \sum_{k,v,c} |\langle \Psi_k^c | \hat{u} \cdot r | \Psi_k^v \rangle|^2 \delta(E_k^c - E_k^v - E), \quad (1)$$

where *c* and *v* are band indexes, Ω is the volume of the system, and $\hat{u}$ is the vector defining the polarization of the incident electric field. $\varepsilon_2(\omega)$ can be thought of as detailing the real transitions between occupied and unoccupied electronic states. Since the dielectric constant describes a causal response, the real and imaginary parts are linked by a Kramers–Kronig transform [17]

$$\varepsilon_1(\omega) - 1 = \frac{2}{\pi} P \int_0^\infty \frac{\omega' \varepsilon_2(\omega') \mathrm{d}\omega'}{\omega'^2 - \omega^2} \quad \text{and}$$

$$\varepsilon_2(\omega) = -\frac{2\omega}{\pi} P \int_0^\infty \frac{\varepsilon_1(\omega') \mathrm{d}\omega'}{\omega'^2 - \omega^2} \quad (2)$$

where *P* means the principal value of the integral. This transform is used to obtain the real part of the dielectric function, $\varepsilon_1(\omega)$.

3. Results and discussion

3.1. Structural description for $La_2Ba(Te_3O_8)(TeO_3)_2$

$La_2Ba(Te_3O_8)(TeO_3)_2$ represents the first lanthanide–alkaline earth mixed metal tellurium(IV) oxide. Its crystal structure features a three-dimensional network in which $[La_2Ba(TeO_3)_2]^{4+}$ layers are cross-linked by $Te_3O_8^{4-}$ anions (Fig. 1).

There are one unique lanthanum(III) atom, one barium(II) and three tellurium(IV) atoms in the asymmetric unit of $La_2Ba(Te_3O_8)(TeO_3)_2$. La(1) is eight-coordinated by eight oxygen atoms from four TeO_3^{2-} and three $Te_3O_8^{4-}$ anions in a square anti-prismatic geometry. It should be mentioned that one of TeO_3^{2-} anions chelates with La(1) bidentately. The La–O distances range from 2.420(7) to 2.657(6) Å (Table 2), which are comparable to those reported in other lanthanum tellurium(IV) oxides [10d,18]. Ba(1) is octahedrally coordinated by six oxygen atoms from four TeO_3^{2-} and two $Te_3O_8^{4-}$ anions, all of which in a unidentate fashion. The Ba–O distances range from 2.730(6) to 2.784(6) Å. There are also four weak Ba–O contacts longer than 3.0 Å, which can be considered as secondary coordination bonds. Te(1) and Te(3) are coordinated by three oxygen atoms in a distorted ψ-TeO_3 tetrahedral geometry with the lone pair of Te(IV) occupying the pyramidal site, whereas Te(2) is coordinated by four oxygen atoms in a distorted ψ-TeO_4 tetragonal pyramidal geometry with the fifth site occupied by the lone pair electrons of the Te(IV). One $Te(2)O_4$ and two $Te(1)O_3$ groups are interconnected via corner-sharing (O(3)) into a $Te_3O_8^{4-}$ anion. The Te–O distances for the Te–O–Te bridges (1.893(6)–2.179(7) Å) are longer than the remaining Te–O bonds (1.827(7)–1.891(6) Å) (Table 2). Such $Te_3O_8^{4-}$ anion has also been reported in $Sm_2MnTe_5O_{13}Cl_2$, which also contains additional $Te_4O_{10}^{4-}$ anion [10e]. In addition to $Te_3O_8^{4-}$ and $Te_4O_{10}^{4-}$ anions, the Te(IV) ion also forms some other oligomers such as $Te_2O_6^{4-}$ anion in $CeTe_2O_6$ and linear $Te_4O_{11}^{6-}$ anion in $Ln_2Te_4O_{11}$ (Ln = La–Lu) [1,9a–d]. Furthermore, the $Te(IV)O_x$ ($x = 3, 4, 5$) groups also can form infinite structures under some special conditions, as exampled by the layered $Te_2O_5^{2-}$ in $Ln(Te_2O_5)X$ (Ln = Nd, X = Cl, Br; Ln = Gd, X = Cl) [2a–b], layered $Te_6O_{13}^{2-}$ in MTe_6O_{13} (M = Mn, Ni, Co) [2c], 1D $Te_7O_{17}^{6-}$ anion in $Cd_7Cl_7(Te_7O_{17})$ and $Te_6O_{13}^{2-}$

anion in $[Cd_2(Te_6O_{13})][Cd_2Cl_6]$ [2d], layered $Te_4O_9^{2-}$ in $K_2Te_4O_9 \cdot 3.2H_2O$ and 3D $Te_2O_6^{4-}$ in $KGaTe_2O_6$ [3]. Bond valence calculations indicate that all Te atoms are +4, the calculated total bond valences for Te(1), Te(2) and Te(3) are 3.99, 3.98 and 4.03, respectively [19].

The interconnection of La^{3+} ions and Ba^{2+} ions by $Te(3)O_3$ groups led to $[La_2Ba(TeO_3)_2]^{4+}$ layers passing through about 1/4 and 3/4 of the *a*-axis (Fig. 2). The interlayer distance is about 9.5 Å. These 2D layers are further interconnected by bridging $Te_3O_8^{4-}$ anions into a 3D network. The lone pairs of the Te(IV) ions are oriented toward the voids of the structure (Fig. 1).

3.2. IR, TGA and optical properties

IR studies indicated that $La_2Ba(Te_3O_8)(TeO_3)_2$ are transparent in the range of 4000–1000 cm^{-1}. The absorption bands at 788, 755, 726, 687 and 616 cm^{-1} are characteristic of *v*(Te–O) vibrations, and band at 439 cm^{-1} is originated from *v*(Te–O–M) vibrations.

Thermogravimetric analysis (TGA) under static air atmosphere indicates that $La_2Ba(Te_3O_8)(TeO_3)_2$ is stable up to 775 °C (See Supporting Materials). It exhibits one main step of weight loss in the temperature range of 775–1300 °C, which corresponds to the release of TeO_2. The observed total weight loss is 49.9% and the final residuals are not characterized.

The absorption spectrum of $La_2Ba(Te_3O_8)(TeO_3)_2$ exhibits a strong absorption peak at about 255 nm (4.87 eV). The emission spectrum of $La_2Ba(Te_3O_8)(TeO_3)_2$ shows two emission bands at around 377 and 417 nm under the excitation at 236 nm (See Supporting Materials). The band-gap determined from optical diffusion reflectance spectrum is 3.81 eV (See Supporting Materials). The emission energies of 3.29 eV (377 nm) and 2.98 eV (417 nm) are less than the optical absorption edge of 3.81 eV (326 nm). Hence, the emission bands of $La_2Ba(Te_3O_8)(TeO_3)_2$ probably originated from defects or excitons [20c,21].

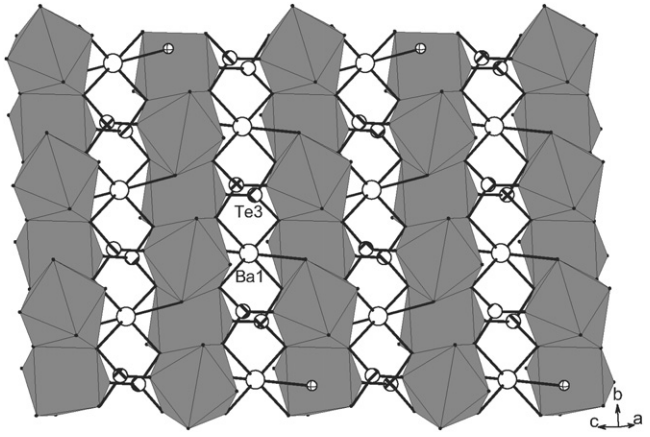

Fig. 2. A $[La_2Ba(TeO_3)_2]^{4+}$ layer in $La_2Ba(Te_3O_8)(TeO_3)_2$. The LaO_8 polyhedra are shaded in middle gray. Ba, Te and O atoms are represented by open (large), hatched and crossed circles, respectively.

3.3. Theoretical studies

The calculated band structure of $La_2Ba(Te_3O_8)(TeO_3)_2$ along high symmetry points of the first Brillouin zone is plotted in Fig. 3, where the labeled *k*-points are present as *L* (−0.5, 0.0, 0.5), *M* (−0.5, −0.5, 0.5), *A* (−0.5, 0.0, 0.0), *G* (0.0, 0.0, 0.0), *Z* (0.0, −0.5, 0.5), and *V* (0.0, 0.0, 0.5). It is found that both the top of valence bands (VBs) and the bottom of conduction bands (CBs) display a small dispersion. The state energies (eV) of the lowest conduction band (L–CB) and the highest valence band (H–VB) at some *k*-points of the crystal $La_2Ba(Te_3O_8)(TeO_3)_2$ are listed in Table 3. The lowest energy (2.97 eV) of conduction bands (CBs) is localized at the *A* point whereas the highest energy (0.00 eV) of valence bands (VBs) is localized at the *G* point. Hence, $La_2Ba(Te_3O_8)(TeO_3)_2$ is an indirect band-gap semiconductor. The calculated indirect band gap of 2.97 eV is smaller than the experimental value of 3.81 eV. The discrepancy is due to the limitation of DFT method that generally underestimates the band gap in semiconductors and insulators [20]. As a result, a scissors operator of 0.8 eV was applied for the calculations of DOS as well as optical properties of $La_2Ba(Te_3O_8)(TeO_3)_2$.

The total and partial densities of states (DOS) are plotted in Fig. 4. The regions below the Fermi level (the Fermi level is set at the top of the valence band) contain 130 bands (two formula units/primitive cell) and can be divided into four regions. The states of Ba-5s, 6s form the VBs lying near −25.0 eV and the VBs ranging from −19.80

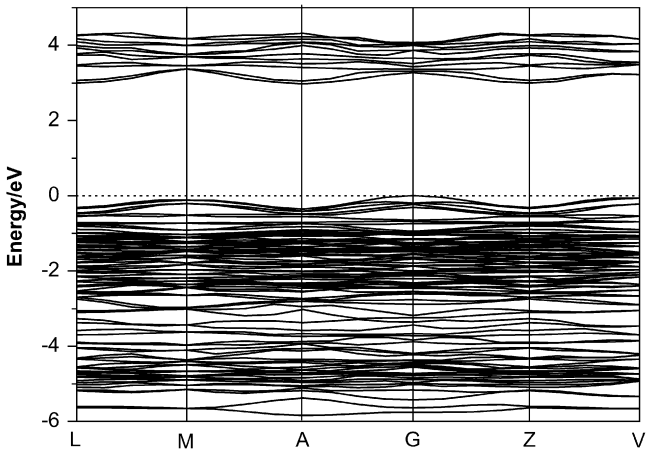

Fig. 3. Band structure of $La_2Ba(Te_3O_8)(TeO_3)_2$ in the range from −6.0 to 5.0 eV. The Fermi level is set at 0.0 eV.

Table 3
The state energies (eV) of the lowest conduction band (L–CB) and the highest valence band (H–VB) at some *k*-points of the crystal $La_2Ba(Te_3O_8)(TeO_3)_2$

k-point	*L*	*M*	*A*	*G*	*Z*	*V*
L–CB	3.00125	3.36775	2.97030	3.26993	3.00125	3.22368
H–VB	−0.31431	−0.11306	−0.35495	0	−0.31430	−0.06052

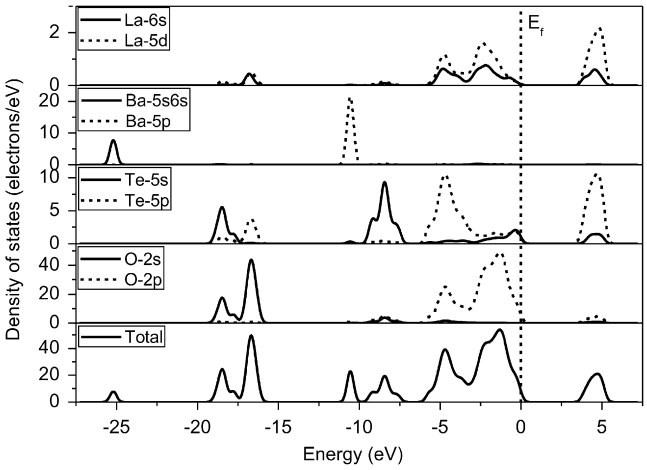

Fig. 4. Total and partial DOS of $La_2Ba(Te_3O_8)(TeO_3)_2$.

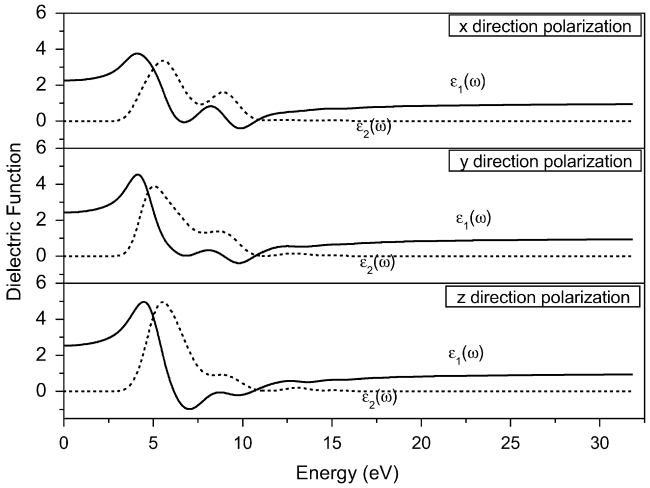

Fig. 5. Calculated real and imaginary parts of dielectric functions of $Ba(Te_3O_8)(TeO_3)_2$ in different polarization directions.

to −15.35 eV are composed of the states of Te-5s, Te-5p, O-2s with small mixings of La-5d and La-6s. The VBs from −11.20 to −7.0 eV are dominated by Ba-5p and Te-5s states. The fourth region of the VBs between −6.50 eV and the Fermi level (0.0 eV) is formed by the O-2p, Te-5s, Te-5p mixing with small amount of O-2s, La-5d and La-6s states. The VBs just below the Fermi level are mainly from O-2p states mixing with a small amount of the Te-5s, Te-5p, confirming the σ(Te–O) bonding interactions. The CBs in the range of 2.88 and 6.05 eV are mostly contributions from Te-5p with a small amount of the O-2p, Te-5s, La-5d and La-6s states.

The chemical bonding properties are also evident from the population analysis. The calculated bond orders for Te–O (1.827(7)–1.893(6) Å) are in the range of 0.42–0.49. Te–O bond with 2.179(7) Å has a much smaller bond order of 0.17. The bond orders for the La–O and Ba–O interactions are in the range of 0.14–0.36 and 0.06–0.09, respectively. Hence, it is concluded that the covalent character of the Te–O bond is significantly larger than that of the La–O bond, and the ionic character of the Ba–O bond is much larger than that of the La–O bond.

Now, to evaluate and assign the observed absorption spectra, we examine the linear optical response properties of $La_2Ba(Te_3O_8)(TeO_3)_2$ crystal, the calculated imaginary part $\varepsilon_2(\omega)$ and the real part $\varepsilon_1(\omega)$ of the frequency-dependent dielectric function with the DFT scissor-operator approximation 0.8 eV are shown in Fig. 5. It is found from the dispersion of the calculated $\varepsilon_2(\omega)$ spectra that the maximum absorption peaks are localized at about 5.56 eV (223 nm), 5.05 eV (246 nm), and 5.53 eV (225 nm) in x, y, and z polarization directions, individually. These are compared with the observed spectrum localized at about 4.87 eV, which is contribution from the charge transfers from O-2p to Te-4p and La-5d states according to the above DOS analysis. We noted that the absorption peaks localize at lower energy for the powders than the crystals and the UV transparent widths are smaller for the powders compared to these of the crystals, which means that the result of the calculation is reasonable [21]. The crystal shows no absorption when the wavelength is larger than 388 nm or photon energy is less than 3.20 eV. As mentioned earlier, the observed ultraviolet edge of cut-off is at about 360 nm for polycrystalline power sample. Therefore, our calculated value is reasonable.

Dielectric constant is an important optical property. It is a measurement of how fast light travels in a medium. The lower is the dielectric constant, the faster the speed of light. The calculated dielectric constants of static case $\varepsilon(0)$ are about 2.2516, 2.4268, and 2.5391 in x, y, and z directions, respectively. The dispersion curves of refractive index are also calculated by the relation of $n^2(\omega) = \varepsilon(\omega)$, and the refractive indexes of n_x, n_y, and n_z are 1.52, 1.58, and 1.62 at a wavelength of 1064 nm, respectively. The refractive index of $La_2Ba(Te_3O_8)(TeO_3)_2$ crystal has not been measured and reported, and therefore, our calculated results can only compare with the observed results of the other tellurite. It is reported that the observed refractive index of tellurite glass is generally 2.1 at 400–700 nm [22]. Comparing with other tellurite glasses, our calculated refractive index in the range of 400–700 nm of the tellurite crystal $La_2Ba(Te_3O_8)(TeO_3)_2$ may be underestimated about 19%.

4. Conclusion

In conclusion, the synthesis, crystal structure and characterization of $La_2Ba(Te_3O_8)(TeO_3)_2$ have been described. $La_2Ba(Te_3O_8)(TeO_3)_2$ features a 3D structure composed of lanthanum barium tellurite layers interconnected by $Te_3O_8^{4-}$ anions. It is observed that the sharp absorption peak is at about 255 nm, which mainly originates from charge transfer from O-2p to Te-4p and La-5d states. $La_2Ba(Te_3O_8)(TeO_3)_2$ is a wide band gap semiconductor with a indirect band gap of 3.81 and 2.97 eV, respectively, based on experimental measurements

and band structure calculations. We are currently exploring other lanthanide alkaline earth tellurium(IV) oxides which may display novel structures and interesting luminescent properties.

Acknowledgments

This work was supported by National Natural Science Foundation of China (nos. 20573113 and 20521101) and NSF of Fujian Province (no. E0420003). We thank Dr. Jing Zhu for the fruitful discussion concerning the DFT calculation.

Appendix A. Supplementary materials

Supplementary data associated with this article can be found in the online version at doi:10.1016/j.jssc.2007.04.002

References

[1] (a) M.S. Wickleder, Chem. Rev. 102 (2002) 2011 (and references therein);
(b) V.P. Verma, Thermochim. Acta 327 (1999) 63 (and references therein).
[2] (a) G.B. Nikiforov, A.M. Kusainova, P.S. Berdonosov, V.A. Dolgikh, P. Lightfoot, J. Solid State Chem. 146 (1999) 473;
(b) S.F. Meier, T. Schleid, Z. Anorg. Allg. Chem. 629 (2003) 1575;
(c) J.T.S. Irvine, M.G. Johnston, W.T.A. Harrison, Dalton Trans. (2003) 2641;
(d) H.L. Jiang, J.G. Mao, Inorg. Chem. 45 (2006) 717.
[3] (a) K.-M. Ok, P.S. Halasyamani, Chem. Mater. 13 (2001) 4278;
(b) P.S. Halasyamani, Chem. Mater. 16 (2004) 3586.
[4] (a) H.-S. Ra, K.-M. Ok, P.S. Halasyamani, J. Am. Chem. Soc. 125 (2003) 7764;
(b) J. Goodey, K.-M. Ok, J. Broussard, C. Hofmann, F.V. Escobedo, P.S. Halasyamani, J. Solid State Chem. 175 (2003) 3;
(c) K.-M. Ok, P.S. Halasyamani, Inorg. Chem. 43 (2004) 4248;
(d) K.-M. Ok, J. Orzechowski, P.S. Halasyamani, Inorg. Chem. 43 (2004) 964.
[5] (a) R.T. Hart, K.-M. Ok, P.S. Halasyamani, J.W. Zwanziger, Appl. Phys. Lett. 85 (2004) 938;
(b) Y. Porter, P.S. Halasyamani, J. Solid State Chem. 174 (2003) 441;
(c) J. Goodey, J. Broussard, P.S. Halasyamani, Chem. Mater. 14 (2002) 3174.
[6] (a) W.T.A. Harrison, L.L. Dussack, A.J. Jacobson, J. Solid State Chem. 125 (1996) 234;
(b) M.G. Johnston, W.T.A. Harrison, Inorg. Chem. 40 (2001) 6518;
(c) V. Balraj, K. Vidyasagar, Inorg. Chem. 38 (1999) 5809;
(d) V. Balraj, K. Vidyasagar, Inorg. Chem. 38 (1999) 3458.
[7] (a) R. Becker, M. Johnsson, R. Kremer, P. Lemmens, Solid State Sci. 5 (2003) 1411;
(b) M. Johnsson, K.W. Törnroos, F. Mila, P. Millet, Chem. Mater. 12 (2000) 2853;
(c) M. Johnsson, K.W. Törnroos, P. Lemmens, P. Millet, Chem. Mater. 15 (2003) 68;
(d) M. Johnsson, S. Lidin, K.W. Törnroos, H.-B. Bűrgi, P. Millet, Angew. Chem. Int. Ed. 43 (2004) 4292.
[8] (a) J. Wontcheu, T. Schleid, J. Solid State Chem. 171 (2003) 429;
(b) M. Ruck, P. Schmidt, Z. Anorg. Allg. Chem. 629 (2003) 2133;
(c) J. Wontcheu, T. Schleid, Z. Anorg. Allg. Chem. 629 (2003) 1463;
(d) I. Krugermann, M.S. Wickleder, J. Solid State Chem. 167 (2002) 113;
(e) I. Krugermann, M.S. Wickleder, Z. Anorg. Allg. Chem. 628 (2002) 147.
[9] (a) I. Ljjaali, C. Flaschenrien, J.A. Ibers, J. Alloy Compd. 354 (2003) 115;
(b) F.A. Weber, S.F. Meier, T. Schleid, Z. Anorg. Allg. Chem. 627 (2001) 2225;
(c) J. Wontcheu, T. Schleid, Z. Anorg. Allg. Chem. 628 (2002) 1941;
(d) Y.L. Shen, J.G. Mao, J. Alloy Compd. 385 (2004) 86;
(e) S.F. Meier, F.A. Weber, R.J. Glaser, T. Schleid, Z. Anorg. Allg. Chem. 627 (2001) 2448;
(f) Y.-L. Shen, H.-L. Jiang, J. Xu, J.-G. Mao, K.-W. Cheah, Inorg. Chem. 44 (2005) 9314.
[10] (a) M.S. Wickleder, M.B. Hamida, Z. Anorg. Allg. Chem. 629 (2003) 556;
(b) W.T.A. Harrison, Z.H. Zhang, J. Solid State Chem. 133 (1997) 572;
(c) R. Berrigan, B.M. Gatehouse, Acta Crystallogr. C 52 (1996) 496;
(d) K.M. Ok, L. Zhang, P.S. Halasyamani, J. Solid State Chem. 175 (2003) 264;
(e) Y.-L. Shen, J.-G. Mao, Inorg. Chem. 44 (2005) 5328.
[11] (a) M.L. Lopez, I. Alvarez, M. Gaitan, A. Jerez, C. Pico, M.L. Veiga, Solid State Ionics 63 (1993) 599;
(b) M.L. Lopez, M.L. Veiga, C. Pico, J. Mater. Chem. 4 (1994) 547;
(c) M.L. Lopez, A. Jerez, C. Pico, R. Saez-Puche, M.L. Veiga, J. Solid State Chem. 105 (1993) 19.
[12] W.M. Wendlandt, H.G. Hecht, Reflectance Spectroscopy, Interscience, New York, 1966.
[13] CrystalClear ver. 1.3.5. Rigaku Corp., Woodlands, TX, 1999; G. M. Sheldrick, SHELXTL, Crystallographic Software Package, SHELXTL, Version 5.1, Bruker-AXS, Madison, WI, 1998.
[14] M. Segall, P. Linda, M. Probert, C. Pickard, P. Hasnip, S. Clark, M. Payne, Materials Studio CASTEP version 2. 2, 2002.
[15] M. Segall, P. Linda, M. Probert, C. Pickard, P. Hasnip, S. Clark, M. Payne, J. Phys.: Condens. Mater. 14 (2002) 2717.
[16] (a) D.R. Hamann, M. Schluter, C. Chiang, Phys. Rev. Lett. 43 (1979) 1494;
(b) M. H. Lee, Ph.D. Thesis, Cambridge University, 1996;
(c) J.S. Lin, A. Qteish, M.C. Payne, V. Heine, Phys. Rev. B 47 (1993) 4174.
[17] J.R. Macdonald, M.K. Brachman, Rev. Mod. Phys. 28 (1956) 393.
[18] S.F. Meier, T. Schleid, Z. Anorg. Allg. Chem. 59 (2004) 881.
[19] (a) N.E. Brese, M. O'Keeffe, Acta Crystallogr. B 47 (1991) 192;
(b) I.D. Brown, D. Altermat, Acta Crystallogr. B 41 (1985) 244.
[20] (a) R.W. Godby, M. Schluther, L.J. Sham, Phys. Rev. B 36 (1987) 6497;
(b) C.M.I. Okoye, J. Phys.: Condens. Matter 15 (2003) 5945;
(c) J. Zhu, W.-D. Cheng, D.-S. Wu, H. Zhang, Y.-J. Gong, H.-N. Tong, D. Zhao, Inorg. Chem. 46 (2007) 208.
[21] J. Zhu, W.-D. Cheng, D.-S. Wu, H. Zhang, Y.-J. Gong, H.-N. Tong, D. Zhao, Eur. J. Inorg. Chem. (2007) 285.
[22] (a) S. Inoue, A. Nukui, K. Yamamoto, T. Yano, S. Shibata, M. Yamane, J. Non-Cryst. Solids 324 (2003) 133;
(b) E. Yousef, M. Hotzel, C. Rűssel, J. Non-Cryst. Solids 342 (2004) 82.